

大型客车侧墙薄板结构焊接变形的数值模拟

闫俊霞，王 军，赵晨阳，刘丽敏*
(河北科技大学 材料学院, 石家庄 050018)



闫俊霞

摘 要: 铁路客车侧墙薄板结构的焊接变形主要是焊后失稳变形, 通过选择包括连续焊、电铆焊、断续焊和塞焊代表性的区域, 利用热—弹塑性数值模拟与解析法相结合的方法, 计算薄板结构的焊后失稳变形. 结果表明, 横向加强筋和纵向加强筋与薄板连接时所采用的断续焊和塞焊工艺是产生薄板失稳变形的主要原因. 薄板自由边的存在明显降低失稳载荷, 增大失稳变形量. 对焊接变形进行了实地测量, 模拟结果与测量结果相吻合, 说明数值模拟具有可靠性.

关键词: 客车侧墙; 数值模拟; 失稳变形

中图分类号: TG404 文献标识码: A 文章编号: 0253—360X(2009)05—0109—04

0 序 言

客车侧墙是机车车辆的重要组成部分, 是一种典型的加筋薄板焊接结构, 在制造过程中容易出现失稳变形. 它的制造质量不仅影响车身外观的美观, 而且对高速客车的空气动力学性能造成影响. 矫正变形费工费时、提高成本, 在矫正中或矫正后还会引起一些新的问题^[1, 2]. 因此, 分析、测量、预测并采取相应措施以控制和调整焊后变形十分重要.

文中采用双经纬仪空间坐标测量系统, 对大型焊接薄板结构焊后变形进行了现场测量. 目的在于测量焊后面外变形并分析引起面外变形的可能原因. 对大型客车侧墙薄板结构经断续焊和塞焊以后薄板的失稳变形, 进行了三维数值模拟. 三维数值模拟与解析法相结合, 即通过数值—解析法, 预测了失稳变形值. 计算结果与实测值基本吻合. 采用模拟方法可提供在各种不同参数和条件下焊接变形的有用信息和参考数据, 从而为控制薄板构件在焊接中的失稳变形提供依据.

所用钢材为耐候钢. 侧墙板为将纵向加强筋(横梁)以及横向加强筋(立柱)放置在不同位置, 与薄钢板焊成最终尺寸, 成为侧墙钢结构. 客车侧墙局部图如图 1 所示. 为了减小或消除薄板平面外变形, 纵向加强筋与横向加强筋均采用 CO₂ 气体保护焊, 并采用断续焊和塞焊的方法, 以减小焊接热输入. 焊角尺寸为 2.5~4.0 mm.

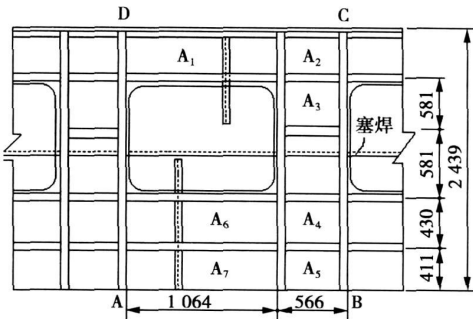


图 1 侧墙局部结构及尺寸示意图(mm)

Fig 1 Sketch schech of local structure on side-wall

1 客车侧墙焊接失稳变形有限元预测

1.1 有限元模型的建立

侧墙整个结构尺寸为 25 m×2.439 m×2.5 mm.

由于实际侧墙结构尺寸很大, 而焊缝尺寸(主要为断续焊和塞焊)又很小, 若对整个结构建立有限元模型显然十分困难. 为了简化计算过程和减少计算工作量, 在进行焊接温度场和热—弹塑性残余应力计算时, 选择测量区域(图 1ABCD 区域)的局部范围(如区域 A₁~A₇)作为研究对象并建立计算模型. 此

收稿日期: 2008—04—11
*参加此项研究工作的还有胡云岩

外,还建立了横向对接板断续焊模型和两列纵向搭接板电铆焊模型. A₇ 区域包含了断续焊、塞焊和直通焊三种薄板结构的典型焊接形式,可以较全面地考察焊接方法对薄板结构变形的影响.

整个有限元计算过程中所用的单元为 8 节点块单元,并采用 2×2 高斯积分法,厚度方向仅分一层.依据具体结构尺寸确定模型单元数量在 510~1 110 之间,节点数为 558~1 178 之间,单元最小尺寸由塑性变形区宽度确定.边界条件:对电铆焊和横向对接断续焊缝,计算区域边界基本为自由,仅在几个节点处施加简支;对 A₁~A₄ 和 A₆ 区域为四边简支,A₅ 和 A₇ 为三边简支一边自由.

1.2 失稳变形计算

首先,利用等效热载荷的思想,即温度载荷作用在三维模型上产生的残余应力分布与二维模型的残余应力分布相同^[3],求得热载荷 ΔT_{app}.其次,定义一个由热载荷 ΔT_{app}所作用区域上的载荷 P_{app},它由弹性模量 E,载荷作用的横截面积 b_pt (b_p 为纵向残余应力拉伸区宽度,t 为板厚),线膨胀系数 α_t 和温度载荷 ΔT_{app} 构成,即

$$P_{app}=Eb_p t \alpha_t \Delta T_{app} \tag{1}$$

板的临界失稳载荷 P_{cr} 定义为

$$P_{cr}=\lambda^{\circ} P_{app} \tag{2}$$

式中:λ 为屈曲载荷乘子,当 0<λ<1 时,薄板结构发生失稳变形,即焊接失稳变形产生的判据为

$$P_{app} \geqslant P_{cr} \tag{3}$$

最后,求焊接失稳变形^[4] 为

$$\frac{\sigma_x}{\sigma_{cr}}=\lambda_0+\lambda_2 W_m^2+\lambda_4 W_m^4 \tag{4}$$

式中:σ_x 为板中部平均压应力;σ_{cr} 为四边简支板的临界失稳应力;λ₀, λ₂ 和 λ₄ 为与板的尺寸、板长度和宽度方向的半波数以及初始挠度有关的参数;W_m 为最大挠度.

进行三维弹性静载失稳计算,考虑以下施焊工序:(1)第一道工序,侧墙板拼接加垫板处对接断续焊缝的影响:断续焊缝沿板横向在计算区域(2 100 mm×1 220 mm)中间.(2)第二道工序,搭接处施行电铆焊的影响:电铆焊点沿板纵向在计算区域(2 510 mm×2 440 mm)的中部.(3)第三道工序,针对加筋梁和立柱支撑框形成的(A₁~A₇)局部区域(图 1)确定断续焊和塞焊的影响,具体计算区域为:A₁(1 072 mm×321 mm),A₂(370 mm×321 mm),A₃(370 mm×452 mm),A₄(370 mm×290 mm),A₅(370 mm×341 mm),A₆(1 072 mm×290 mm),A₇(1 072 mm×341 mm);由于具体结构尺寸、约束及焊接参数不同,施加于焊缝上的热载荷有所不同,但最终形成的等效残余应力场尽量保证与实际一致.使用 AIGOR FEAS 有限元程序进行弹性屈曲分析时,材料密度为 7.8 g/mm³,杨氏模量 E=260 GPa,泊松比取 0.3,线膨胀系数 α_t=1.2×10⁻⁵/℃,重力加速度 g=9.8 m/s².不同条件下临界失稳载荷乘子及失稳评定结果如表 1 所示.

表 1 不同区域失稳评定结果
Table 1 Bucking judgement results on different selected areas

计算区域	尺寸(mm)	屈曲载荷乘子 λ= P _{cr} / P _{app}	板中部平均压应力 σ _x /MPa	最大挠度计算结果 W _m /mm	失稳评定结果
对接断续焊 ^①	2 100×1 220×2.5	-0.066 383	—	—	不失稳
电铆焊 ^②	2 510×2 440×2.5	-0.146 501	—	—	不失稳
No. 1 :A ₁ ^③	1 072×321×2.5	0.645 634	77	3.2	失稳
No. 2 :A ₂ ^③	370×321×2.5	0.563 597	87	3.7	失稳
No. 3 :A ₃ ^③	370×452×2.5	0.668 137	59	2.9	失稳
No. 4 :A ₄ ^③	370×290×2.5	0.765 307	38	2.3	失稳
No. 5 :A ₅ ^③	370×341×2.5	0.754 123	62	4.5	失稳
No. 6 :A ₆ ^③	1 072×290×2.5	0.757 912	100	2.3	失稳
No. 7 :A ₇ ^③	1 072×341×2.5	0.195 340	45	15.2	失稳

注:①第一道工序计算模型;②第二道工序计算模型 ③第三道工序计算模型

2 数值结果分析与讨论

根据实际焊接工艺参数进行焊接残余应力有限元数值模拟,计算得出塞焊的塑性区宽度为 35 mm,断续焊的塑性区宽度为 40 mm.

计算结果表明,由于横向焊接方向尺寸(1.22 m)明显小于板纵向尺寸(25 m),断续焊缝不会产生失稳,屈曲载荷乘子 λ=P_{cr}/ P_{app}≤0 表示在焊缝区施加热载荷才会出现失稳;实际上沿两列侧墙薄板中间搭接处电铆焊,为每间隔 1 064 mm(该区域为窗口,最后要切割掉)在长 510 mm 区域进行电

铆焊, 由于围绕电铆焊缝周围很大区域(上下各为 1 220 mm, 前后为 1 050 mm)对焊缝的约束作用, 其电铆焊的焊缝及其周围区域也不会失稳; 施焊完加筋梁和立柱后(第三道工序), 每块加筋框中均出现失稳($0 \leq \lambda = P_{cr}/P_{app} \leq 1$)现象, 局部板形状愈趋于正方形面积愈大, 板的临界载荷愈低(如 A₃, $\lambda = 0.668\ 137$), 自由边的存在将显著降低板的临界载荷(如 A₇, $\lambda = 0.195\ 340$ 为最小), 应尽量采用封闭的加筋框结构。

由表 1 可看出, 预测最大挠度在 2.3~15.2 mm 之间, 板较长(A₁ 和 A₆), 挠度并不一定较大, 仅达 2.3~3.2 mm, 这是因为板越长, 在长度方向可形成多个半波形(A₁ 和 A₆ 分别形成 3 个半波形), 从而降低了变形量。而带自由边的长板变形最大, 为 15.2 mm。必须强调, 上述计算并未考虑初始板不平度的影响, 一般而言, 初始不平度将增大变形量。总之, 失稳分析表明, 侧墙的焊接屈曲变形是比较严重的, 必须采取有效措施加以控制。

3 客车车体侧墙焊接变形的测量与数据处理

3.1 焊接变形的测量

采用双经纬仪空间坐标测量系统对薄板结构的焊接变形进行了测量^[5], 该方法的测量原理是两台经纬仪一旦固定, 空间坐标系即建立起来, 就可获得空间点的统一坐标值。

为了避免测量重复, 取一具代表性单元, 该区域含原始薄钢板的对接部分, 经过对已焊车体侧墙的观察, 该区域估计焊接变形最为严重。被测区域尺寸如图 1 中的 ABCD 区域。

变形的测量是在侧墙拼焊成最终尺寸后进行的。被测点选取 54 个, 均匀布置在图 1 中的 ABCD 区域, 测量的原始数据为被测点的水平角 α 和竖直角 β 。经转化, 最终为被测点的三维坐标值, 即点 (x, y, z) 值。

3.2 测量数据分析与处理

如果实际薄板平面不受焊接变形等因素的影响, 那么其理想板面应该是一个平面。可用平面方程来描述, 但实际平面显然存在初始变形与焊接变形。根据形位公差国家标准的规定^[6], 平面度误差是指被测表面对理想平面的变动量, 而理想平面的方位应符合最小条件。采用最小二乘法, 用平面来逼近变形的曲面。设理想的平面方程为

$$z = ax + by + c$$

(5)

即逼近已知点 $(x_1, y_1, z_1), (x_2, y_2, z_2) \cdots (x_k, y_k, z_k)$ 的最小二乘平面方程为

$$ax_k + by_k - z_k + c = 0$$

(6)

依据最小二乘法原理, 设

$$\phi(a, b, c) = \sum_{k=1}^m (ax_k + by_k + c - z_k)^2$$

(7)

式中: m 为被测的点数, 则

$$\left\{ \begin{aligned} \left(\sum_{k=1}^m x_k^2 \right) a + \left(\sum_{k=1}^m x_k y_k \right) b + \left(\sum_{k=1}^m x_k \right) c &= \sum_{k=1}^m x_k z_k \\ \left(\sum_{k=1}^m x_k y_k \right) a + \left(\sum_{k=1}^m y_k^2 \right) b + \left(\sum_{k=1}^m y_k \right) c &= \sum_{k=1}^m y_k z_k \\ \left(\sum_{k=1}^m x_k \right) a + \left(\sum_{k=1}^m y_k \right) b + mc &= \sum_{k=1}^m z_k \end{aligned} \right.$$

(8)

以上方程称为最小二乘平面的法方程组。常量 a, b 和 c 可通过式(8)确定。实际测点到理想平面的距离 d 为

$$d = \frac{|ax_k + by_k - z_k + c|}{\sqrt{a^2 + b^2 + 1}}$$

(9)

由式(9)求得被测点 (x_k, y_k, z_k) 到拟合平面的距离。在拟合平面两侧, 各取被测点到拟合平面的最大距离, 其和即为所测区域的不平度, 记为 W 。利用实际测量点在理想平面上的投影点 (x_k, y_k) 坐标值和对应点的计算值 d_i (被测点 (x_k, y_k, z_k) 到拟合平面的距离), 经适当拟合可获得被测实际平面相对于理想平面的曲面形状如图 2 所示。

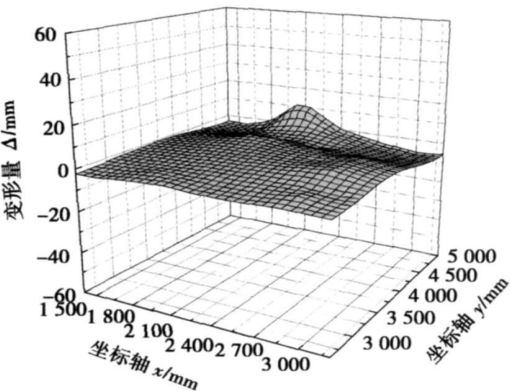


图 2 曲面变形图
Fig 2 Bucking distortion pattern

依据求得的被测点到拟合平面的距离的结果, 并根据国内传统的客车侧墙焊后不平度的测量方案(其方案为用 1 m 尺在侧墙进行“米字”型测量, 配合塞规, 得出侧墙的不平度), 取约 1 m×1 m 的范围, 求出其范围的不平度, 所取计算范围见图 3, 各范围的不平度如表 2 所示。

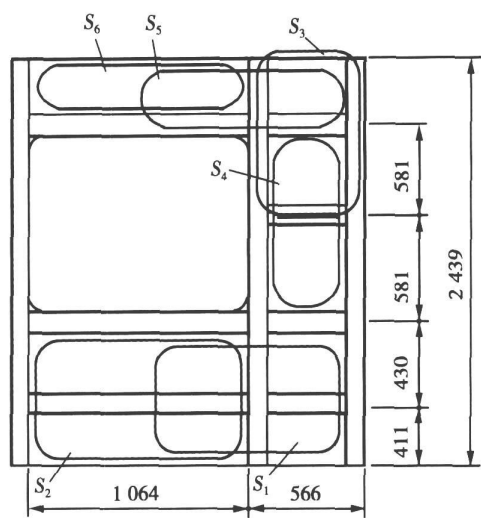


图 3 确定不平度所定义的局部区域(mm)
Fig. 3 Defined local areas for getting side wall roughness

表 2 局部区域的不平度计算结果

Table 2 Measured results of side wall roughness at local areas

测量区域	S_1	S_2	S_3	S_4	S_5	S_6
变形量 Δ /mm	17.8	15.2	5.7	5.5	2.5	2.3

将表 2 的测量结果与表 1 的数值模拟结果进行比较,从比较的结果可以看出,最大残余变形的吻合较好.这表明对这类薄板结构采用模拟—解析相结合的大变形分析方法是可行的,而且计算也十分简捷.

4 结 论

(1) 采用数值—解析相结合的方法对大型客车

侧墙薄板焊接失稳变形进行了分析,其结果与实测值吻合良好,表明所用的分析方法可行.

(2) 客车侧墙薄板结构组装时对接焊缝和电铆焊不会造成薄板的失稳,而横向加强筋和纵向加强筋与薄板连接时的断续焊和塞焊将产生薄板失稳变形.

(3) 客车侧墙板为自由边的区域,焊接变形最大.建议将自由边设计为带有加强筋的形式,以提高失稳变形荷载,减小薄板的失稳变形.

参考文献:

[1] Mollicone P, Camilleri D, Gray T G F, *et al.* Simple thermo-elastic-plastic models for welding distortion simulation[J]. Journal of Materials Processing Technology, 2006, 176(3): 77—86.

[2] Tekriwal P, Mazumder J. Transient and residual thermal strain-stress analysis of GMAM[J]. Transactions of ASME, 1991, 113(6): 336—343.

[3] 闫俊霞, 霍立兴, 张玉凤, 等. 焊接薄板失稳变形预测方法[J]. 焊接学报, 2005, 26(6): 50—53.

Yan Junxia, Huo Lixing, Zhang Yufeng, *et al.* Approach of predicting welding buckling deformation of thin plate[J]. Transactions of the China Welding Institution, 2005, 26(6): 50—53.

[4] 陈铁云, 沈惠中. 结构的屈曲[M]. 上海: 上海科学技术文献出版社, 1993.

[5] 罗 明. 移动式空间坐标测量系统的研究[D]. 天津: 天津大学, 1996.

[6] 董 竟. 几何量测量[M]. 北京: 机械工业出版社, 1992.

作者简介: 闫俊霞, 女, 1964 年出生, 博士, 副教授. 主要从事焊接结构残余应力和焊接变形的数值模拟研究. 发表论文 10 余篇.

Email: yanjx@hebust.edu.cn

structured light image of weld seam

Elimination of gas holes of laser cladding on 2A12 aluminum alloys

SUN Fujuan (Qingdao Branch, Naval Aeronautical Engineering Academy, Qingdao 266041, Shandong, China). p93–96

Abstract: Laser cladding Al-Y (6% Y) was used to repair corrosion damage of 2A12 aluminum alloys. One group of the specimens was shocked on every deposited layer, the other was only deposited Al-Y (6% Y). After aging and fatigue test, fracture and element test were studied. The results show that the safety life of the shocked specimen is 871% of the specimens without shock and there was no pore in the deposited layer which is joined firmly with the substrate. There were many pores in the deposited layer of the specimens without shock, which lead to reduction of the safety life. The element test indicates that parts of the substrate is engaged in metalurgical procedure and the element Y is seriously burnt.

Key words: aluminum alloys; laser cladding; safety life; fatigue fracture

Experiment research on laser transmission welding of two different thermoplastics

WANG Xiao, YANG Kun, ZHANG Huizhong, LIU Huixia (School of Mechanical Engineering, Jiangsu University, Zhenjiang 212013, Jiangsu, China). p97–100

Abstract: The experiments on laser transmission welding of dissimilar plastic between transparent PS and PVC were carried out with clearweld additive, and the welding quality was investigated by orthogonal test. Tensile and section tests were conducted for experimental samples, and the influence of welding factors on tensile strength and weld seam size were analyzed. The optimized welding parameters are obtained by range method, which indicates the influencing parameters on welding strength are welding speed, fixture pressure, beam diameter, laser average power, laser frequency, holding time after welding. Research results are helpful to guide practical production.

Key words: laser welding; polystyrene; polyvinylchloride; additive; transmission welding

Digital AC servo push & pull feeding system for CO₂ welding

YANG Shuai, LIU Jia, YAN Sibo, YIN Shuyan (College of Mechanical Engineering & Applied Electronics Technology, Beijing University of Technology, Beijing 100124, China). p101–104

Abstract: A push & pull feeding system with real-time control for CO₂ welding was proposed and achieved. It utilizes the motion controller to control AC servo motor with the low moment of inertia, fast response, and the buffer to connect the constant feeding part and the push & pull feeding part. The PWM feeder speed control circuit with speed negative feedback by rotate coder was designed to compensate the speed fluctuation caused by the system load and sup-

ply voltage changing. The push & puller feeding mechanism was designed to push & pull the wire based on the AC servo motor. According to the characteristics of CO₂ welding with push & pull feeding system, the feeder speed curve is pre-designed. The wire motion was managed by the real-time control software written in the motion controller. The system has good ability in anti-jamming and stability. The highest feeder frequency with push & pull process can reach 90 Hz.

Key words: AC servo motor; buffer; real-time control; push & pull feeding

SPH simulation on agglomerate Fe particle deposition in low temperature high velocity air fuel spraying process

Genliang¹, XU Xin², YUAN Xiaojing¹ (1. The Second Artillery Engineering College 501 staff, Xi'an 710025, China; 2. The Second Artillery Equipment Research Institute, Beijing, 100085, China). p105–108

Abstract: In order to study the effect of the agglomerate metal particle on the coatings building-up, the agglomerate nano metal particle deposition characteristics with smoothed particle hydrodynamics (SPH) were simulated in low temperature high velocity air fuel (LTHVAF) thermal spraying process. The results show that the agglomerate particles are splashed when the agglomerate particles impact on the substrate. During the deposition process, the effective strain of agglomerate particle is larger than that of the micron particle, but the area ratio of the agglomerate particle is less. At the same time, the pervasion occurs when the metal particle impacts on the substrate, which increases with the particle velocity.

Key words: thermal spray; nano-agglomerate particle; deposition characteristics; numerical simulation

Numerical simulation of welding deformation of a large carriage side wall

YAN Junxia, WANG Jun, ZHAO Chenyang, LIU Limin (College of Materials, Hebei University of Science and Technology, Shijiazhuang 050018, China). p109–112

Abstract: The main welding deformation of railway carriage sidewall was welded buckling distortion, which was simulated by thermal elastic-plastic finite element method with analysis in several selected areas including continuous welds, plug welds and intermittent welds. The results show that the plug welding and intermittent welding are the main reason that induce bucking distortion of sidewall in which transverse stiffeners and longitudinal stiffeners are welded on the side-wall. The critical bucking load decreases obviously and the bucking distortion increases on the plate with a free boundary. The measured results of bucking distortion are in agreement with the simulation results. Thus, a complete set of instruction can be received for the real processing.

Key words: carriage side-wall; numerical simulation; buckling distortion